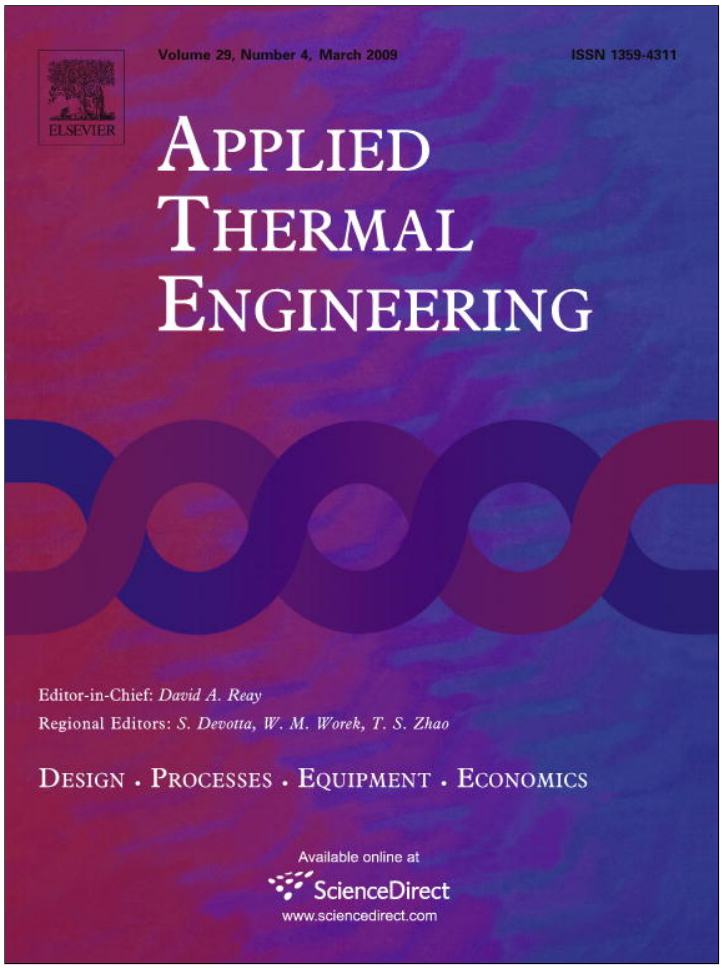

Applied Thermal Engineering 29 (2009) 770–778

Contents lists available at ScienceDirect

Applied Thermal Engineering

journal homepage: www.elsevier.com/locate/apthermeng

Performance of a residential heat pump operating in the cooling mode with single faults imposed

Minsung Kim [a], W. Vance Payne [b,*], Piotr A. Domanski [b], Seok Ho Yoon [c], Christian J.L. Hermes [d]

[a] Geothermal Energy Research Center, Korea Institute of Energy Research, Daejon 305-343, Korea
[b] Building and Fire Research Laboratory, National Institute of Standards and Technology, Gaithersburg, MD 20899-8631, USA
[c] Energy Systems Research Division, Korea Institute of Machinery and Materials, Daejon 305-343, Korea
[d] POLO Research Laboratories in Cooling and Thermophysics, Federal University of Santa Catarina, 88040-970 Florianopolis-SC, Brazil

ARTICLE INFO

Article history:
Received 12 July 2007
Accepted 4 April 2008
Available online 22 April 2008

Keywords:
Heat pump
Fault detection and diagnosis
Rule-based decision chart
Thermostatic expansion valve

ABSTRACT

The system behavior of a R410A residential unitary split heat pump operating in the cooling mode was investigated. Seven artificial faults were implemented: compressor/reversing valve leakage, improper outdoor air flow, improper indoor air flow, liquid line restriction, refrigerant undercharge, refrigerant overcharge, and presence of non-condensable gas in the refrigerant. This study monitored eight fault detection features and identified the most sensitive features for each fault. The effect of the various fault levels on energy efficiency ratio (EER) was also estimated. Since the studied system employed a thermostatic expansion valve (TXV) as an expansion device, it could adapt to some faults making the fault less detectable. The distinctiveness of the fault depended on the TXV status (fully open or not).

Published by Elsevier Ltd.

1. Introduction

The characterization of vapor compression system faults has been pursued by many investigators. Breuker and Braun [1] surveyed frequently occurring faults for a packaged air conditioner using field data. Based on the field data, Breuker and Braun sorted field faults into three different categories according to the cause of the fault, service frequency, and service cost. Downey and Proctor [2] also collected data on over 13,000 air conditioners in residential and commercial installations. Refrigerant charge and indoor airflow were major factors in the poor performance of the surveyed systems. Sixty-five percent of the residential units in this survey needed additional refrigerant and/or indoor air flow correction.

Only recently have investigators begun to examine FDD techniques for vapor compression systems rather than the broader area of building/HVAC systems FDD. FDD for vapor compression systems was initially intended to help technicians servicing individual vapor compression systems. Grimmelius et al. [3] developed an on-line failure diagnosis system for a vapor compression refrigeration system used in a naval vessel or a refrigerated plant. Stylianou and Nikanpour [4] represented a methodology using thermodynamic modeling, pattern recognition, and expert knowledge to determine the state of a reciprocating chiller and to diagnose selected faults. Rossi and Braun [5] developed a device to diagnose system faults by monitoring temperatures and pressures and applying these measurements to a look-up fault chart. Chen and Braun [6] collected the laboratory data for 17.6 kW (5 ton) rooftop unit with a TXV as an expansion device and imposed artificial faults to the unit for developing two rule-based FDD methods. Smith and Braun [7] performed field tests on a 17.6 kW (5 ton) rooftop unit with a TXV and a 10.6 kW (3 ton) rooftop unit with a fixed orifice expansion device. They proposed a decoupling-based unified FDD technique to handle multiple simultaneous faults. Li [8] re-examined the statistical rule-based method initially formulated by Rossi and Braun [5] and also developed the concept of virtual sensors to estimate characteristic parameters from indirect component modeling. Kim and Kim [9] tested a water-to-water heat pump system with a variable speed compressor and an electrical expansion valve (EEV). They also provided an FDD algorithm along with two different rule-based charts depending on the compressor status. Proctor [10] markets an expert system within a database that uses technician gathered system information to diagnose system faults. All of these investigators are attempting to apply FDD methods to residential and light commercial vapor compression systems.

The objective of the present research was to test a thermostatic expansion valve (TXV) equipped heat pump operating in the cooling mode in order to map system parameters during fault-free and imposed-fault operation. System status was monitored, and performance parameters were recorded. Seven faults were imposed: (i) compressor valve/reversing valve leakage, (ii) improper outdoor air flow, (iii) improper indoor air flow, (iv) liquid line restriction, (v) refrigerant undercharge, (vi) refrigerant overcharge, and (vii) presence of non-condensable gas. A following study will use these collected results for the development of FDD methods.

* Corresponding author. Tel.: +1 301 975 6663; fax: +1 301 975 8973.
E-mail address: vance.payne@nist.gov (W.V. Payne).

1359-4311/$ - see front matter Published by Elsevier Ltd.
doi:10.1016/j.applthermaleng.2008.04.009

Nomenclature

a	coefficient of multivariate polynomial
CF	condenser airflow fouling fault
CMF	compressor/reversing valve leakage fault
cmp	compressor
COP	coefficient of performance
E	uncertainty
EER	energy efficiency ratio (Btu/(W h))
EF	evaporator airflow fouling fault
h	specific enthalpy, kJ/kg (Btu/lbm)
k	specific instant of kth time interval
LL	refrigerant liquid line restriction fault
m_R	refrigerant mass flow rate, kg/h (lbm/h)
n	number of data samples in a moving window
OC	refrigerant overcharge fault
P	pressure, kPa (psia)
Q_{CA}	condenser air-side capacity, W (Btu/h)
Q_{CR}	condenser refrigerant-side capacity, W (Btu/h)
Q_{EA}	evaporator air-side capacity, W (Btu/h)
Q_{ER}	evaporator refrigerant-side capacity, W (Btu/h)
R	residual of features
SEER	seasonal energy efficiency ratio (Btu/(W h))
SHR	sensible heat ratio (−)
T_{CR}	condenser inlet saturation temperature, °C (°F)
T_{DW}	compressor discharge-line wall temperature, °C (°F)
T_{DB}	dry-bulb temperature, °C (°F)
T_{DP}	dewpoint temperature, °C (°F)
T_{ER}	evaporator exit saturation temperature, °C (°F)
T_{ID}	indoor dry-bulb temperature, °C (°F)
T_{IDP}	indoor dew-point temperature, °C (°F)
T_{OD}	outdoor dry-bulb temperature, °C (°F)
ΔT_{CA}	condenser air temperature rise, °C (°F)
ΔT_{EA}	evaporator air temperature drop, °C (°F)
ΔT_{LL}	liquid line temperature drop, °C (°F)
T_{SAT}	refrigerant saturation temperature at a given pressure, °C (°F)
ΔT_{SC}	liquid line subcooling, °C (°F)
ΔT_{SH}	evaporator exit superheating, °C (°F)
UC	refrigerant undercharge fault
v	variance
W_{cmp}	compressor work (W)
W_{tot}	total work (W)
x	measured data
$\bar{x}$	moving window average of measured data

Greek symbols

ϕ	feature or performance parameter
σ	standard deviation

2. Experimental setup

2.1. System description and implementation of artificial faults

The studied system was an R410A 8.8 kW (2.5 ton) split residential heat pump with seasonal energy efficiency ratio (SEER) of 13 [11]. The unit was comprised of the indoor fan-coil section, outdoor section with a scroll compressor, a thermostatic expansion valve (TXV), and connecting tubing. Both the indoor and outdoor air-to-refrigerant heat exchangers were of the finned-tube type. The unit was installed in environmental chambers and charged with refrigerant according to the manufacturer's specifications. Fig. 1 illustrates the experimental setup for FDD tests. Detailed specifications of the test rig including indoor ductwork, dimensions, data acquisition and instrumentations were described in Kim et al. [12].

Table 1 lists the seven types of common faults which were investigated in this study. The presence of non-condensables can result from improper installation while the remaining faults may also result from improper installation or may take place over the heat pump lifecycle. The respective causes may be compressor valve wear, outdoor coil fouling, indoor coil fouling or ice clogging, dirty refrigerant filter/dryer, improper refrigerant recharge service, and refrigerant leakage. These seven faults and their implementation during tests are discussed in more detail in the following sections.

2.2. Experimental procedure and test conditions

A comprehensive test series was carried out to map the performance of the system at normal (fault-free) operation and with imposed faults. Table 2 presents operating conditions for the test program for fault-free tests. Indoor conditions included two temperatures, 21.1 °C (70.0 °F) and 26.7 °C (80.0 °F), and two levels of relative humidity, 50% and dry coil. For outdoor conditions, four temperatures were selected: 21.1 °C (70.0 °F), 27.8 °C (82.0 °F), 32.2 °C (90.0 °F), and 37.8 °C (100.0 °F). Since outdoor relative humidity is not an influential parameter for performance of the condenser, it was controlled roughly around 50% within the range of 40–60%.

The test schedule for fault-free steady-state operation involved 17 different conditions; one ARI 210/240 Standard rating test and 16 full factorial combinations of chamber conditions. The test conditions adopted for the faulty tests are indicated in Table 2 by two asterisks (tests 4, 5, 8, and 9). All fault-free tests were performed twice to check experimental repeatability. In addition, a fault-free test preceded a series of tests carried out for a given fault at each of the four operating conditions.

2.3. Measurement uncertainties

On the refrigerant side, pressure transducers and T-type thermocouple probes were attached at the inlet and exit of every component of the system. The refrigerant mass flow rate was also measured using a Coriolis flow meter. The measurements of temperature, pressure, and mass flow rate took place in the locations indicated in Fig. 1. The air enthalpy method served as the primary measurement of the system capacity, and the refrigerant enthalpy method served as the secondary measurement. These two measurements always agreed within 5%. All uncertainties were calculated at a 95% confidence on the mean value.

As an example, the uncertainty in COP may be calculated from the percent uncertainties listed in Table 3

$$\mathrm{COP} = \frac{Q_{EA}}{W_{tot}} \tag{1}$$

$$E_{COP} = \left[\left(\frac{\partial \mathrm{COP}}{\partial Q_{EA}} dQ_{EA}\right)^2 + \left(\frac{\partial \mathrm{COP}}{\partial W_{tot}} dW_{tot}\right)^2\right]^{\frac{1}{2}} \tag{2}$$

Since the uncertainties in capacity and total power are expressed as percentages of the current value, Eq. (2) simplifies and may be expressed as a relative uncertainty as shown in the following equation:

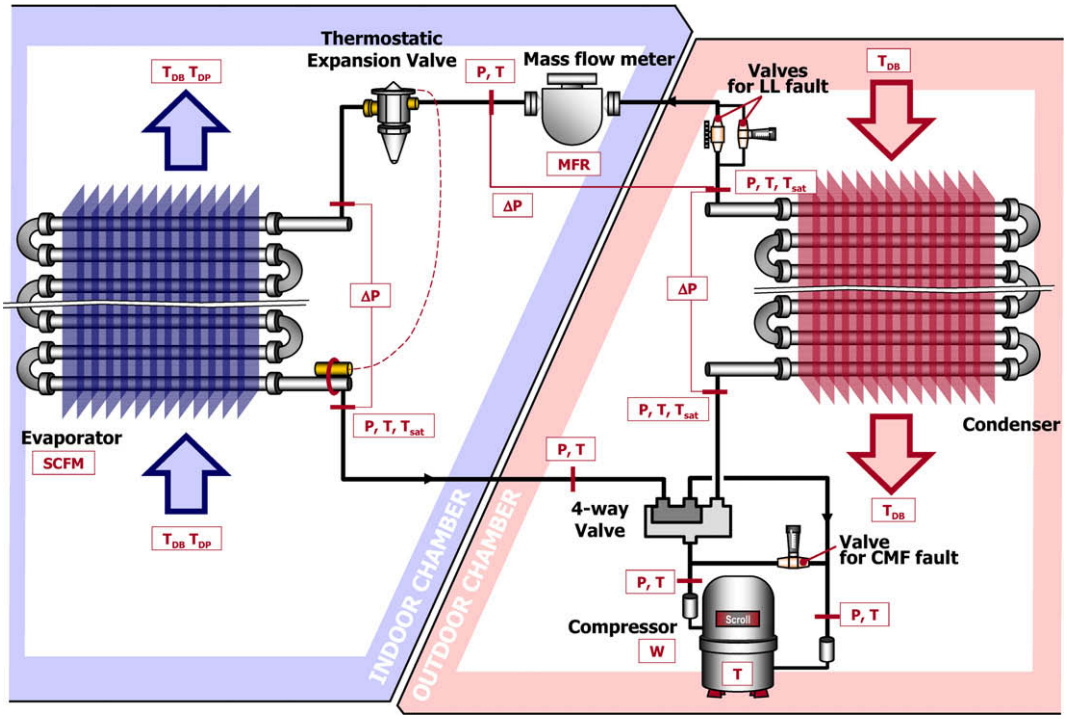

Fig. 1. Experimental setup with the heat pump in the cooling mode.

Table 1
Description of studied faults

Fault	Abbreviation	Determination of level of fault during tests
Compressor leakage (4-way valve leakage)	CMF	% of refrigerant flow rate
Improper outdoor air flow rate	CF	% of coil area blocked
Improper indoor air flow rate	EF	% of air flow rate reduction
Liquid line restriction	LL	% of normal pressure drop through TXV
Refrigerant overcharge	OC	% overcharge from the correct charge
Refrigerant undercharge	UC	% undercharge from the correct charge
Presence of non-condensable gases	NON	% of non-condensable gas with respect to system volume

$$\frac{E_{COP}}{COP} = \sqrt{\left(\frac{E_{W_{cmp}}}{W_{tot}}\right)^2 + \left(\frac{E_{Q_{EA}}}{Q_{EA}}\right)^2} \quad (3)$$

Table 3 lists characteristic uncertainties of the major quantities measured during this work. A very detailed analysis of uncertainty for testing done according to ASHRAE Standard 37 may be found in [13].

3. Performance test results

3.1. Fault-free test results

Fig. 2 presents variation of selected system parameters at different operating conditions. These tests were performed with the aid of a steady-state detector (SSD) as described in Kim et al. [14]. The SSD allowed consistent indication of steady conditions which greatly enhanced the speed at which data were gathered.

Table 2
Operating conditions for fault-free tests

Test number	Indoor		Outdoor	
	Dry-bulb temperature °C (°F)	Relative humidity (%)	Dry-bulb temperature °C (°F)	Relative humidity (%)
1*	26.7 (80.0)	51	35.0 (95.0)	40–60
2	21.1 (70.0)	50	21.1 (70.0)	40–60
3	26.7 (80.0)	50	21.1 (70.0)	40–60
4**	21.1 (70.0)	50	27.8 (82.0)	40–60
5**	26.7 (80.0)	50	27.8 (82.0)	40–60
6	21.1 (70.0)	50	32.2 (90.0)	40–60
7	26.7 (80.0)	50	32.2 (90.0)	40–60
8**	21.1 (70.0)	50	37.8 (100.0)	40–60
9**	26.7 (80.0)	50	37.8 (100.0)	40–60
10	21.1 (70.0)	Dry coil	21.1 (70.0)	40–60
11	26.7 (80.0)	Dry coil	21.1 (70.0)	40–60
12	21.1 (70.0)	Dry coil	27.8 (82.0)	40–60
13	26.7 (80.0)	Dry coil	27.8 (82.0)	40–60
14	21.1 (70.0)	Dry coil	32.2 (90.0)	40–60
15	26.7 (80.0)	Dry coil	32.2 (90.0)	40–60
16	21.1 (70.0)	Dry coil	37.8 (100.0)	40–60
17	26.7 (80.0)	Dry coil	37.8 (100.0)	40–60

* ARI Standard 210/240 (2006).
** Combination of test conditions selected for fault tests.

Fig. 2a shows that the refrigerant superheat at the evaporator exit increases as the outdoor temperature decreases particularly for the test with 26.7 °C (80.0 °F) dry-bulb temperature, where the TXV does not open wide enough to provide enough refrigerant flow at the small pressure differential between the evaporator and condenser. The numeric labels in Fig. 2b represent the test number described in Table 2. As the outdoor temperature increases, the compressor requires more power. However, the compressor power in Fig. 2c is a weak function of the indoor operating conditions; the lines representing compressor power for the four indoor conditions considered in this study nearly overlap each other. The EER plot in Fig. 2d shows some differences due to the differences in evaporator capacities.

Table 3
Measurement uncertainties

Measurement	Range	Total uncertainty at the 95% confidence level
Individual temperature	−18 °C to 93 °C (0–200 °F)	±0.3 °C (±0.5 °F)
Temperature difference	0–28 °C (0–50 °F)	±0.3 °C (±0.5 °F)
Air nozzle pressure	0–1245 Pa (0 in H_2O to 5.0 in H_2O)	±1.0 Pa (±0.004 in H_2O)
Refrigerant mass flow rate	0–544 kg/h (0–20 lbm/min)	±1.0%
Dew-point temperature	0–38 °C (32–100 °F)	±0.4 °C (0.8 °F)
Dry-bulb temperature	1–38 °C (35–100 °F)	±0.4 °C (0.8 °F)
Total power	100–5000 W	3.5%
Total cooling capacity	4.4–10.6 kW (15,000–36,000 Btu/h)	4.0%
Coefficient of performance	2.5–6.0	5.5%

3.2. Fault-free steady-state (FFSS) reference model

The objective of the FFSS tests described above was to take measurements at different environmental operating conditions at different system locations to monitor key systems parameters – referred to as features – and to develop models to correlate these features. The outdoor dry-bulb temperature, T_{OD}, indoor dry-bulb temperature, T_{ID}, and indoor dew-point temperature, T_{IDP}, are the independent variables that define operating conditions. All features, ϕ_i, can be explicitly described by multivariate polynomials correlated to the FFSS data as a function of T_{OD}, T_{ID}, and T_{IDP}. Eq. (4) represents the general formulation of a 2nd order multivariate polynomial equation with crossterms used in this research. Table 4 shows the root mean squared (RMS) error for the model listed in Eq. (4).

$$\phi_i = a_0 + a_1 T_{OD} + a_2 T_{ID} + a_3 T_{IDP} + a_4 T_{OD} T_{ID} + a_5 T_{ID} T_{IDP} + a_6 T_{IDP} T_{OD} + a_7 T_{OD}^2 + a_8 T_{ID}^2 + a_9 T_{IDP}^2 \quad (4)$$

3.3. Performance variation under single faults

The feature residuals were calculated as shown in Eq. (5). The reference value, $\phi_{i,reference}$, was based upon the 2nd order polynomial model shown in Eq. (5) and discussed in Kim et al. [12]

$$R(\phi_i) = \phi_{i,measurements} - \phi_{i,reference} \quad (5)$$

3.3.1. Compressor/reversing valve leakage

The compressor/reversing valve leakage fault (CMF) involved at least three fault levels. The fault level was calculated as the ratio of refrigerant mass flow through the system with the fault imposed divided by the refrigerant mass flow rate during the fault-free operation.

Fig. 3a and b show that the residuals for the refrigerant saturation temperatures, T_{ER} and T_{CR}, have similar responses for all operating conditions. Also, the change in air temperature difference across the evaporator and condenser was similar for the operating conditions studied. This system characteristic corresponds to the similar slopes of the capacity lines for the evaporator in Fig. 3c. W_{cmp} in Fig. 3d slightly decreased with the increasing level of fault because of the corresponding reduction of the temperature (pressure) lift produced by the increased evaporator temperature and decreased condenser temperature.

3.3.2. Improper outdoor air flow rate (condenser fouling)

Fault levels of 5%, 10%, 20%, and 35% were implemented by blocking the corresponding percentage of the finned frontal area of the condenser. The change in T_{ER} is minor, but T_{CR} increases significantly for a higher condenser fouling level. The compressor discharge-line wall temperature, T_{DW}, in Fig. 4a also increases with an increased level of this fault.

Fig. 4c with the residual of the liquid line temperature change, ΔT_{LL}, provides an indication of the lack of refrigerant subcooling, or small subcooling, at the condenser outlet. Since the heat transfer between the liquid line and ambient is typically small, the temperature change in the liquid line is negligible unless two-phase refrigerant is entering the line or refrigerant flashes in the line due to its pressure drop. If the refrigerant is two-phase, the

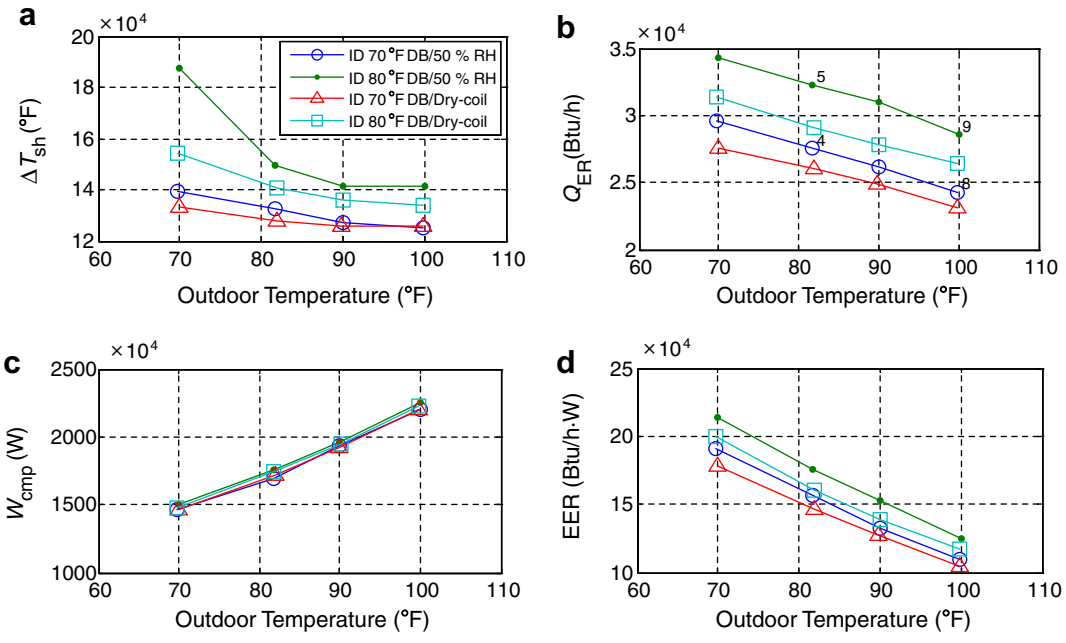

Fig. 2. Variation of system performance under fault-free condition: (a) ΔT_{sh}, (b) Q_{ER}, (c) W_{cmp}, and (d) EER.

Table 4
RMS errors of the 2nd order multivariate polynomial model

Feature	T_E	ΔT_{sh}	T_D	T_C	ΔT_{sc}	ΔT_{EA}	ΔT_{CA}
RMS error °C (°F)	0.168 (0.303)	0.383 (0.689)	0.448 (0.806)	0.071 (0.127)	0.208 (0.374)	0.078 (0.140)	0.171 (0.307)

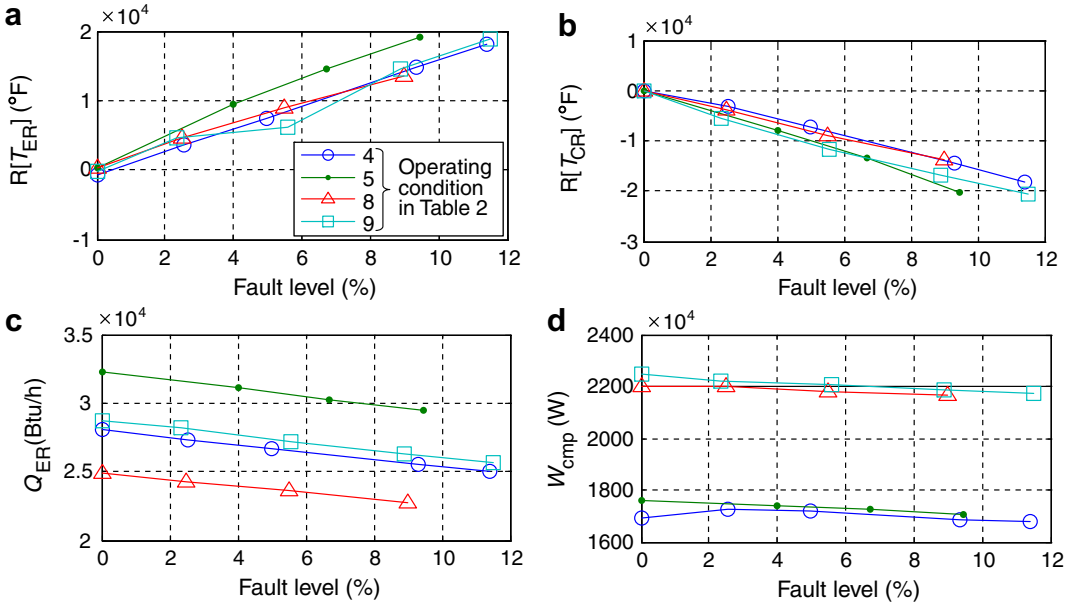

Fig. 3. Variation of system parameters at the compressor/reversing valve leakage fault: (a) residual of T_{ER}, (b) residual of T_{CR}, (c) Q_{ER}, and (d) W_{cmp}.

temperature decreases along the liquid line in proportion to the pressure drop. Fig. 4c with a fault level greater than 10% shows distinct temperature change in the liquid line.

All parameters in Fig. 4 "behave" in a systematic fashion except those associated with Test 5 at 26.7 °C (80.0 °F)/27.8 °C (82.0 °F) indoor/outdoor temperature at 35% fault levels. It can be speculated that during that condition, with greatly reduced condenser air flow, the refrigerant entering the TXV carried a substantial amount of bubbles, where the TXV could not allow sufficient refrigerant mass flow even if it were fully open (actuator saturation). Therefore, EER in Fig. 4d shows more degradation (greater negative slope) at this fault level than at other fault levels.

3.3.3. Improper indoor air flow rate (evaporator fouling)

The improper indoor air flow rate fault was implemented by controlling the speed of the nozzle chamber booster fan located at the end of the ductwork. Reducing the indoor air flow approximates evaporator fouling. The tests included three fault levels at approximately 10%, 20%, and 30%, which corresponded to the respective reductions of the air flow rate from the no-fault condition.

The change in T_{ER} in Fig. 5a is the strongest indication of the reduced air flow. This change is very similar for all four operating conditions used. A change in the air temperature drop across the evaporator, ΔT_{EA}, in Fig. 5b is the second consistent system response for all operating conditions. The condenser saturation temperature also drops uniformly with the increased fault level; however, the temperature drop is only 0.6 °C (1.0 °F) for a 30% reduction in the indoor air flow. Both the sensible and latent capacity change linearly with reduced air flow. The sensible heat ratio (SHR) decreases since more moisture is condensed due to lower air velocity and the reduced evaporator refrigerant saturation temperature.

3.3.4. Liquid line restriction

The restriction fault was implemented by modulating the settings of two valves, as seen in Fig. 1, installed in parallel in the liquid line. The level of the liquid line restriction fault was numerically assigned by the ratio of the increase in the liquid line pressure drop and the pressure differential between the upstream and downstream of the TXV at the no-fault condition.

In a system equipped with a variable opening expansion device – such as a TXV – the expansion device tends to compensate for over-restriction in the liquid line. Consequently, the over-restriction will not change the system performance as long as the expansion device can open enough to maintain refrigerant mass flow rate at the smaller available pressure differential that exists between the expansion device inlet and the inlet to the evaporator. In our case, the TXV was able to compensate for the restriction fault up to approximately a 10% increase in liquid line pressure drop. Only after the restriction exceeded the 10% fault level did the residuals for the selected features start to show a departure from their fault-free values. The fault was most pronounced for ΔT_{sh} and ΔT_{LL} shown in Fig. 6. All of the performance parameters were basically unaffected up to the 10% fault level. Beyond this point, all performance parameters deteriorated.

3.3.5. Refrigerant undercharge and overcharge

The fault level for refrigerant undercharge (or refrigerant overcharge) was calculated as the ratio of the charge reduction (or charge excess) and the optimal refrigerant charge in the system. The test program included six fault levels: ±10%, ±20%, and ±30%, where negative and positive signs represent undercharge and overcharge, respectively. With improper refrigerant charge, ΔT_{sc} (Fig. 7a) is the most indicative of the fault regardless of the operating conditions. A reduced refrigerant charge causes T_{ER} (Fig. 7b) to decrease beginning at a 10% undercharge depending on the operat-

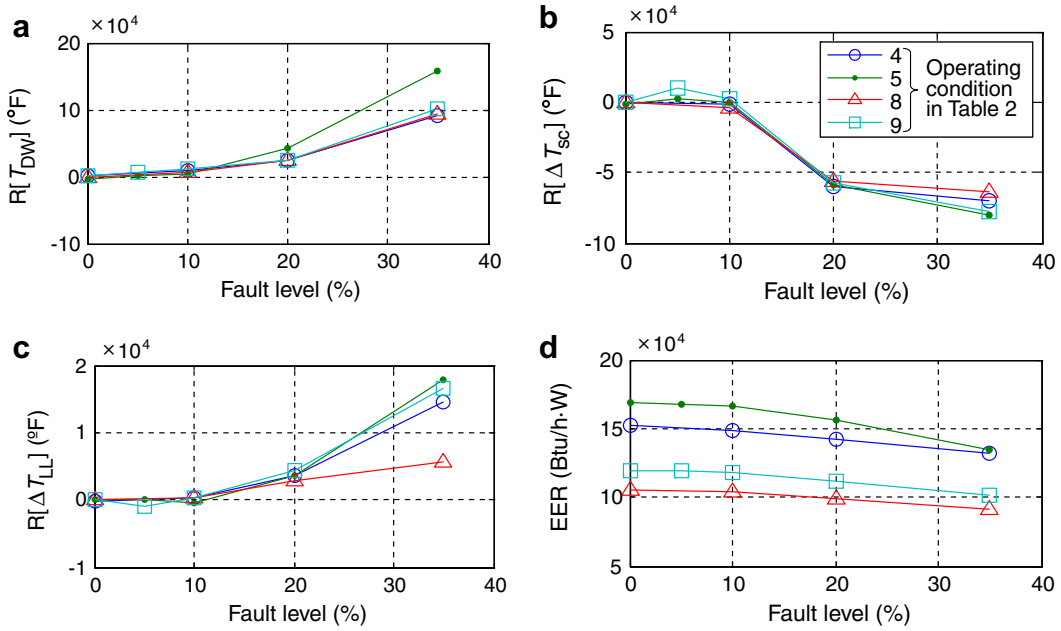

Fig. 4. Variation of system parameters at the improper outdoor coil air flow rate fault: (a) residual of T_{DW}, (b) residual of T_{SC}, (c) residual of ΔT_{SC}, and (d) EER.

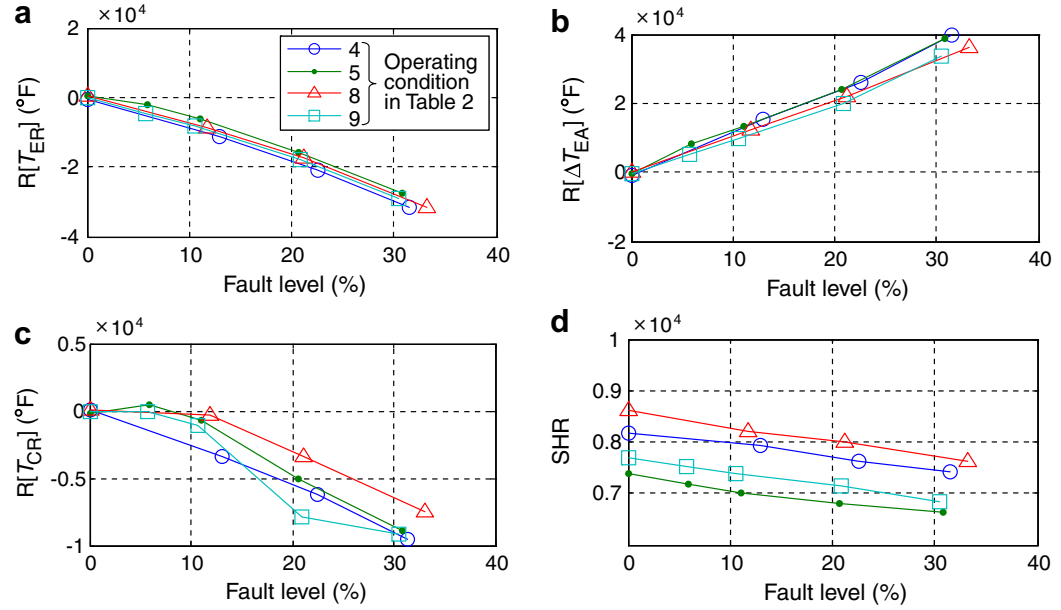

Fig. 5. Variation of system parameters at the improper indoor coil air flow rate fault: (a) residual of T_{ER}, (b) residual of DT_{EA}, (c) residual of T_{CR}, and (d) SHR.

ing conditions. T_{DW} (Fig. 7c) provides non-linear signals with a strong dependence on operating conditions at undercharge fault. The capacity (Fig. 7d) is more affected by undercharging than overcharging. The EER plot (Fig. 7e) has a maximum, which is reached near the optimal refrigerant charge.

3.3.6. Presence of non-condensable gas

This fault was implemented by charging a controlled amount of dry nitrogen into the system. The mass of charged nitrogen divided by the mass of nitrogen that could occupy the system at atmospheric pressure indicated the fault level. It was estimated that a typical level of this fault found in the field installation should not exceed 5%, and for this level we performed tests for all four operating conditions applied to other faults. To include more severe scenarios, we carried out tests at 10%, 15%, and 20% fault levels at two extreme operating conditions of #5 and #8 in Table 2.

The full range of non-condensable gas fault tests was performed at the lowest temperature lift (test #5) and highest temperature lift (test #8) to reduce testing effort; only the 5% fault level was performed at the other conditions. The residuals for ΔT_{sc} (Fig. 8a) provide the strongest and most consistent indication of the increasing level of fault. Equally consistent is the plot for T_{CR} (Fig. 8b). T_{DW} also has a positive trend with the increasing level of fault; however, the collected data have a scatter that typically burdens compressor discharge temperature readings. All of the characteristic features are related to the condenser, which can be explained by the fact that non-condensable gases are likely to accumulate in the condenser. Non-condensables collect on the

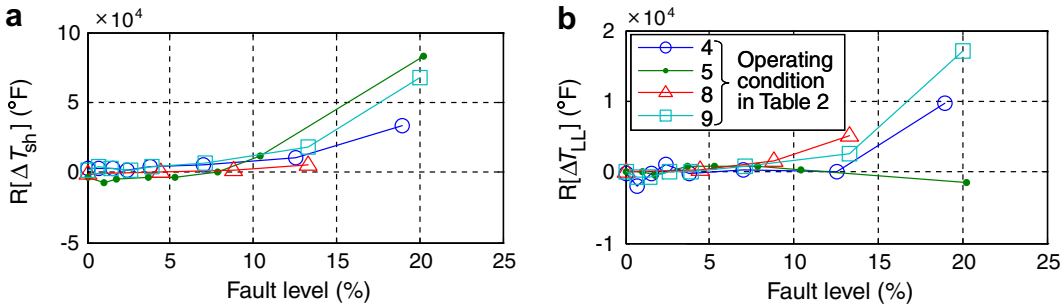

Fig. 6. Variation of system parameters for the liquid line restriction fault: (a) residual of ΔT_{sh} and (b) residual of ΔT_{LL}.

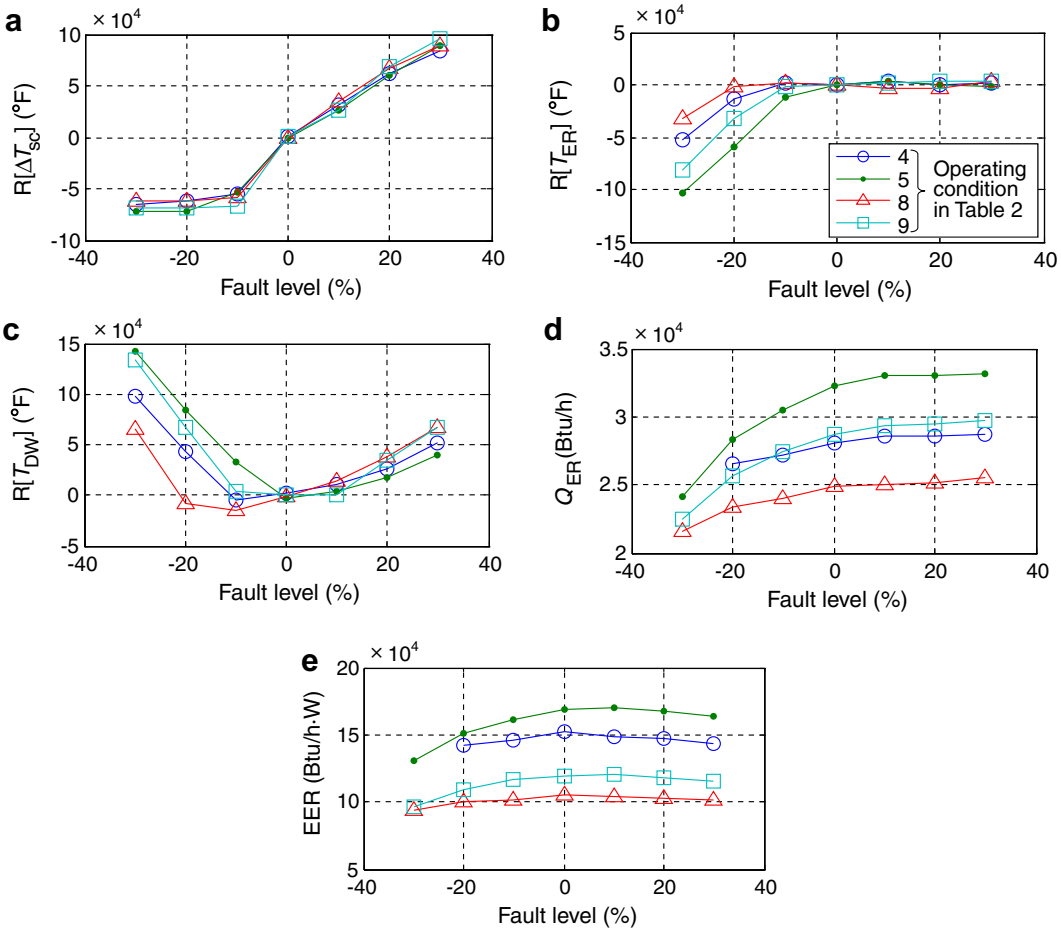

Fig. 7. Variation of system parameters at the improper refrigerant charge fault: (a) residual of ΔT_{sc}, (b) residual of T_{ER}, (c) residual of T_{DW}, (d) evaporator refrigerant-side capacity, and (e) EER.

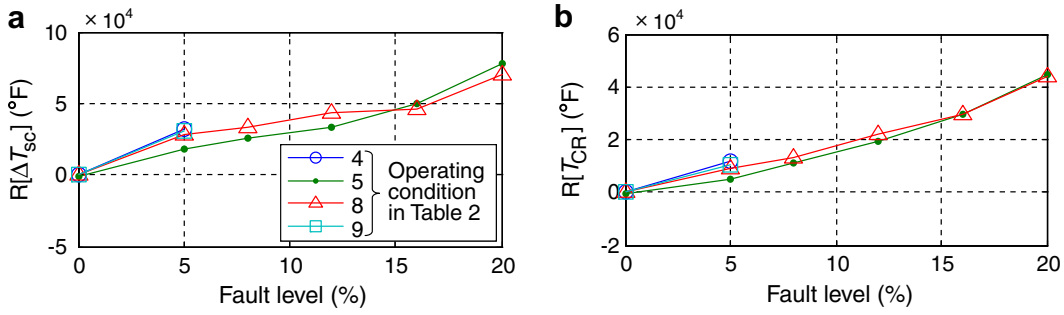

Fig. 8. Variation of system performance at the non-condensable gas fault: (a) residual of ΔT_{sc} and (b) residual of T_{CR}.

high pressure side of the system and raise the condensing pressure above that corresponding to the temperature at which the refrigerant is actually condensing. This increases power consumption and reduces capacity. The excess pressure is caused by the partial pressure of the non-condensables.

4. Comparative evaluation of fault effects

Fig. 9 presents a histogram of estimated fault levels that would cause a 5% reduction in EER relative to the fault-free EER. The bars within the chart marked by an asterisk represent linear extrapolation of fault tests to the level that would cause 5% degradation in EER. When reviewing this figure we should bear in mind that the studied faults were imposed by different methods, and it is difficult to compare the degree of their severity. For example, the measure of fault level for improper outdoor air flow rate (condenser fouling) was the percentage of the coil are blocked, but for the indoor air flow rate (evaporator fouling) it was the actual flow rate reduction.

From the chart, EER is relatively insensitive to evaporator fouling or refrigerant overcharge faults. Since this is a heat pump

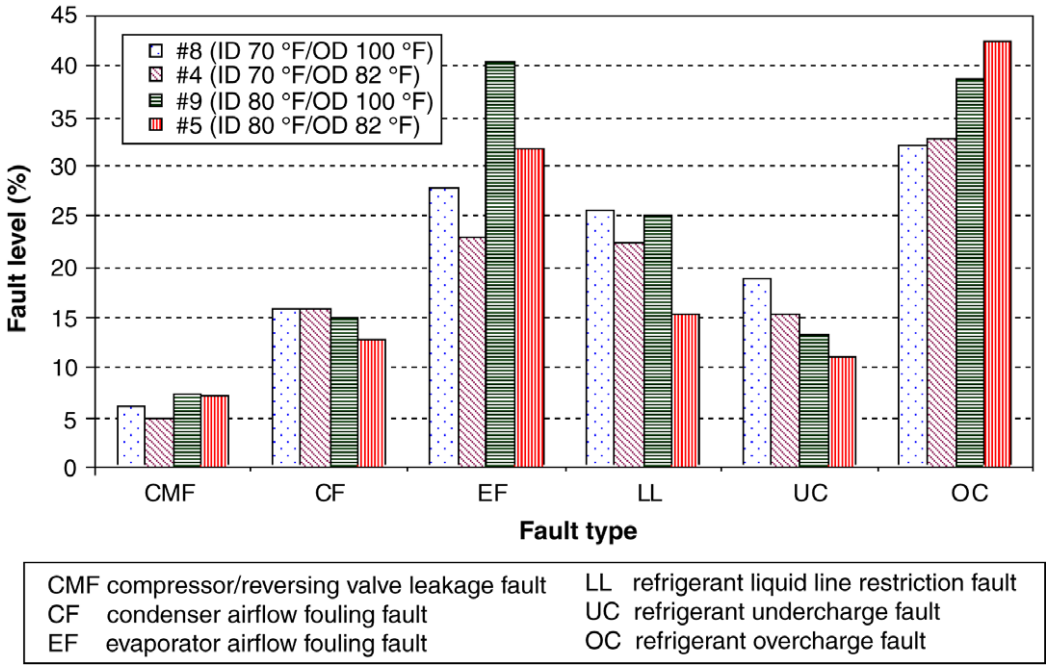

Fig. 9. Estimated fault levels for each fault at a 5% degradation in EER at four different operating conditions.

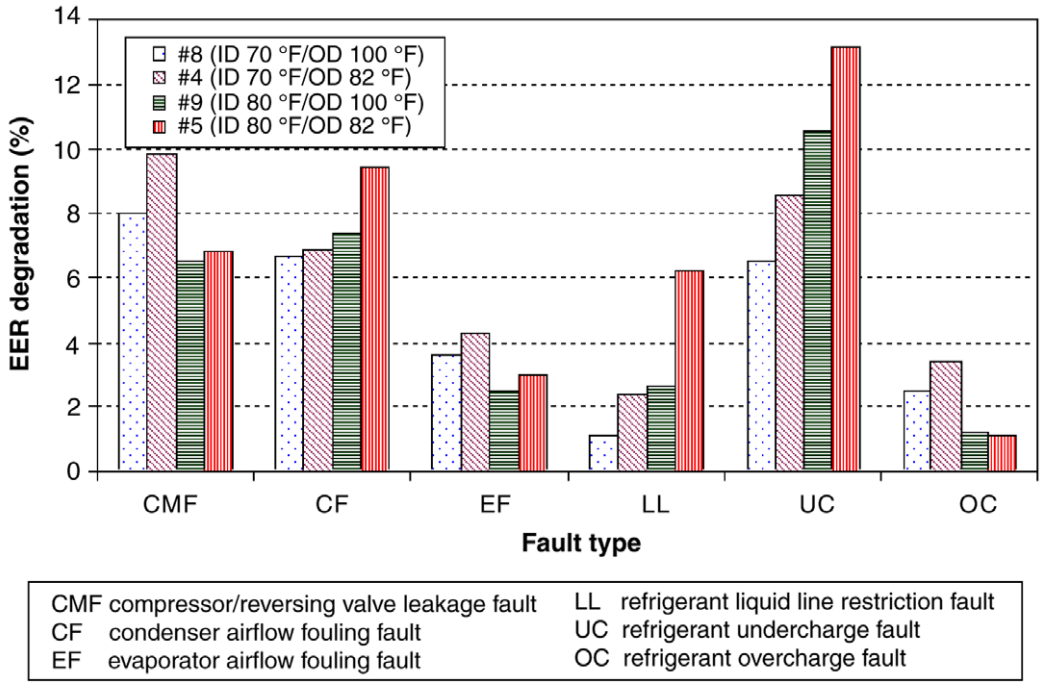

Fig. 10. Estimated EER degradation for 10% level compressor fault and 20% fault level for other faults at four different operating conditions.

Table 5
Most sensitive features to studied single faults

Fault	Feature	Comment
Compressor/reversing valve leakage	T_{CR}, T_{ER}	
Improper outdoor air flow	ΔT_{SC}, T_{DW}, T_{CR}	Only seen after faults greater than 10%
Improper indoor air flow	T_{ER}, ΔT_{EA}	
Liquid line restriction	ΔT_{SH}, ΔT_{LL}, T_{DW}	TXV mitigates this fault until a fault level of greater than 10%
Refrigerant undercharge	ΔT_{SC}, ΔT_{SH}, T_{DW}	EER more affected by undercharge
Refrigerant overcharge	ΔT_{SC}, T_{DW}, T_{CR}	
Non-condensable gas	ΔT_{SC}, T_{CR}, T_{DW}	

system, the evaporator is larger than would be seen in a comparable cooling-only air conditioner; this makes the heat pump system less susceptible to EER degradation due to improper indoor airflow. For refrigerant overcharge, the fault is the most distinctive at the highest temperature lift (indoor and outdoor temperature difference) test #8 showing the low capacity. Fig. 9 indicates that the 5% degradation in EER occurs more readily at the high capacity low lift test #5 than at the low capacity high lift test #8. This trend appears to be true for all faults except evaporator fouling or refrigerant overcharge. All faults, except the compressor leakage fault, must have a fault level greater than 10% to produce a 5% decrease in EER.

Fig. 10 presents estimated EER degradation due to five different faults relative to the fault-free EER. The figure shows that highest EER degradation occurs with a 20% refrigerant undercharge, especially at the lowest temperature lift occurring for test #5. EER degradation due to overcharge is much smaller.

5. Concluding remarks

This paper provides basic information on the behavior of a TXV-equipped R410A residential unitary split heat pump operated in the cooling mode during fault-free and imposed single-fault conditions. Table 5 presents the most sensitive features for each studied fault. Besides detail differences, the results and general trends of data presented in this paper are in agreement with those of Chen and Braun [6] reported for a TXV-equipped 17.6 kW rooftop unit. One of the differences is the selection of features for detecting the improper outdoor air flow fault; Chen and Braun [6] selected the residual of condensing temperature in their Sensitivity Ratio Method, while our study indicated ΔT_{SC} and T_{DW} as the most sensitive features. Our measurements show the residual of condensing temperature to have indeed a clear and consistent trend for all operating conditions studied, however, ΔT_{SC} could indicate an improper condenser air flow at a lower fault level while T_{DW} became a strong fault indicator at the higher level of the fault.

Since the studied system was controlled by a TXV, it could adapt to some faults making the fault less detectable. The distinctiveness of the fault depended on the TXV status (fully open or not). For the tests with liquid line restriction, little degradation of capacity and EER occurred due to the TXV control of superheat. Once the liquid line was restricted to the point at which the TXV was fully open in the attempt to maintain the target superheat, the system response to greater liquid line restriction was typical to that of a fixed-area expansion device system. In this case, a TXV with a larger orifice size would be required to control the superheat, which implies that the fault effect can be influenced by the effective orifice size of the TXV.

Acknowledgements

Lennox Industries in Carrollton, Texas donated the heat pump system used in this study. The authors also thank Mr. Robert Uselton and all of his co-workers at Lennox for giving us their time and advice during several meetings. Seok Ho Yoon's research at the National Institute of Standards and Technology, Gaithersburg, MD, was supported by a Korea Research Foundation Grant funded by the Korean Government (MOEHRD, KRF-2005-214-D00240). C.J.L. Hermes duly acknowledges the CAPES Agency, Government of Brazil, for supporting his sabbatical stay at NIST.

References

[1] M.S. Breuker, J.E. Braun, Common faults and their impacts for rooftop air conditioners, HVAC&R Research 4 (3) (1998) 303–318.
[2] T. Downey, J. Proctor, What can 13,000 air conditioners tell us? in: Proceedings of the 2002 ACEEE Summer Study on Energy Efficiency in Buildings, Paper 431, Panel 1, ACEEE Publications, 1001 Connecticut Ave, NW, Suite 801, Washington, DC 20036, 2002.
[3] H.T. Grimmelius, J.K. Woud, G. Been, On-line failure diagnosis for compression refrigeration plants, International Journal of Refrigeration 18 (1) (1995) 31–41.
[4] M. Stylianou, D. Nikanpour, Performance monitoring, fault detection, and diagnosis of reciprocating chillers, ASHRAE Transactions 102 (Part 1) (1996) 615–627.
[5] T.M. Rossi, J.E. Braun, A statistical rule-based fault detection and diagnostic method for vapor compression air conditioners, HVAC&R Research 3 (1) (1997) 19–37.
[6] B. Chen, J.E. Braun, Simple rule-based methods for fault detection and diagnostics applied to packaged air conditioners, ASHRAE Transactions 107 (Part 1) (2001) 847–857.
[7] V.A. Smith, J.E. Braun, Fault detection and diagnostics for rooftop air conditioners, Final Report Compilation for Project 2.1, Publication #P500-03-096, California Energy Commission, 2003, <http://www.archenergy.com/cec-eeb/reports.htm>.
[8] H. Li, A decoupling-based unified fault detection and diagnosis approach for packaged air conditioners, Ph.D. Thesis, Purdue University, West Lafayette, IN, 2004.
[9] M. Kim, M.S. Kim, Performance investigation of a variable speed vapor compression system for fault detection and diagnosis, International Journal of Refrigeration 28 (4) (2005) 481–488.
[10] J. Proctor, CheckMe!™ Expert Analysis System Developed by Proctor Engineering Group, 418 Mission Avenue, San Rafael, CA 94901, <http://www.proctoreng.com/checkme/checkme.html>, 2006.
[11] ARI Standard 210/240-2006, Standard for Unitary Air Conditioning and Air Source Heat Pump Equipment, Air Conditioning and Refrigeration Institute, Fairfax, VA.
[12] M. Kim, W.V. Payne, P.A. Domanski, C.J.L. Hermes, Performance of a Residential Heat Pump Operating in the Cooling Mode with Single Faults Imposed, NISTIR 7350, National Institute of Standards and Technology, Gaithersburg, MD, USA, 2006.
[13] W.V. Payne, P.A. Domanski, Muller, A Study of a Water-to-Water Heat Pump Using Hydrocarbon and Hydrofluorocarbon Zeotropic Mixtures, NISTIR 6330, National Institute of Standards and Technology, Gaithersburg, MD, USA, 1999.
[14] M. Kim, S.H. Yoon, W.V. Payne, P.A. Domanski, Design of a steady-state detector for fault detection and diagnosis of a residential air conditioner, International Journal of Refrigeration, doi:10.1016/j.ijrefrig.2007.11.008.